http://dx.doi.org/10.5935/0103-5053.20160037

J. Braz. Chem. Soc., Vol. 27, No. 9, 1577-1586, 2016.
Printed in Brazil - ©2016 Sociedade Brasileira de Química
0103 - 5053 $6.00+0.00

Article

Novel Non Enzymatic TBHQ Modified Electrochemical Sensor for Hydrogen Peroxide Determination in Different Beverage Samples

Navid Nasirizadeh,[a,b] Masoud Ghaani,[c] Zahra Shekari[a] and Mohammad Shateri-Khalilabad[b]*

[a]*Scientific Society of Nanotechnology,* [b]*Department of Textile and Polymer Engineering and* [c]*Department of Food Science and Technology, Yazd Branch, Islamic Azad University, Yazd, Iran*

A nanosensor was developed for hydrogen peroxide determination based on nafion/graphene oxide/silver nanoparticles/tertiary butylhydroquinone (TBHQ) modified glassy carbon electrode (N-GO/AgNPs/TBHQ/GCE). Cyclic voltammetry was used to investigate the electrochemical behavior of this modified electrode and differential pulse voltammetry was used for the reduction of H_2O_2. The limit of detection was 0.46 μmol L^{-1} and three linear calibration ranges were obtained for H_2O_2 determination from 1.52-9.79 μmol L^{-1} for first linear segment, 9.79-231.0 μmol L^{-1} for second linear segment and 231.0-8330.0 μmol L^{-1} for third linear segment. Finally, the reliability of the nanosensor was confirmed in the real sample analysis in different beverages with satisfactory results.

Keywords: hydrogen peroxide, tertiary butylhydroquinone (TBHQ), graphene oxide, silver nanoparticle, electrocatalytic reduction

Introduction

tert-Butylhydroquinone (TBHQ) is a well-known food-grade antioxidant, which has been applied as an efficient preservative for unsaturated vegetable oils, abundant meat products and edible animal fats at low concentrations (less than 0.02%).[1] The presence of TBHQ does not change the flavor, odor and color of the material which it is added to.[2] This compound is a derivative of hydroquinone by substitution of *tert*-butyl group. Numerous surface modified electrodes with compounds containing a hydroquinone moiety have been studied. Modified electrodes with hydroquinone can be used in the studying of electrocatalytical oxidation or reduction of different materials such as hydrogen peroxide (H_2O_2).

H_2O_2 forms during catalyzed reactions by different oxidase in many biological and environmental processes.[3] This compound regards as an elemental key in many different applications such as clinical, chemical, biological, food production and also it is widely used in pulp and paper bleaching, sterilization and many other industries.[4] Especially in food industry, H_2O_2 is used for sterilizing and cleaning equipments applied for mixing, transporting and packing.[3] The other aspect of H_2O_2 importance is in diary industry. This compound is known as an antibacterial agent in milk and it should be removed by the use of some catalase before milk to cheese microbiological transformation.[5] Also, H_2O_2 is often produced as a by-product of some enzyme reactions, hence knowledge about reaction forward is up to determine the amount of produced H_2O_2.[6] Thus determination of this compound has a great point of interest. Many methods have been used for determination of H_2O_2 such as chemiluminescence,[7] chromatography,[8] fluorimetric[9] and spectrophotometric.[10] However electrochemical sensors based on chemically modified electrodes were known as more reliable, selective and sensitive method with lower cost and ease of use and fast response time.[11]

From the analytical point of view direct reduction of H_2O_2 at bare electrode is not working properly because of low kinetic and high over potential necessary for H_2O_2 reduction on different electrode materials.[12] Applying modified electrodes equipped with appropriate electrocatalyst such as hydroquinone derivative, is one way to deal with this problem and decrease the over-potential for H_2O_2 reduction reaction.[4] In addition, various enzymes are widely used for H_2O_2 determination because of its good sensitivity and selectivity.[13] But most of them are not environmentally stable and these are quite expensive.[14] In

*e-mail: nasirizadeh@yahoo.com

consequence, number of studies were done on the use of non-enzymatic sensors to decrease their limit of detection and extend their respond range.[15]

Recently, noble nanomaterials have been widely used in analytical electrochemistry due to their high surface area, excellent biocompatibility, good conductivity and adsorption ability.[16] Silver nanoparticles (AgNPs) is one of these nanomaterials that used as catalyst in different reactions.[17] Graphene oxide (GO) is another nanomaterial that applied for modification of electrode surfaces because of its large surface area, perfect conductivity, excellent chemical stability and easy fabrication.[18]

In this paper an enzyme free electrochemical sensor was fabricated based on the immobilization of TBHQ on silver nanoparticles deposited on graphene oxide and used for determination of H_2O_2 concentration. The electrochemical behavior of nafion/graphene oxide/silver nanoparticles/TBHQ modified glassy carbon electrode (N-GO/AgNPs/TBHQ/GCE) is investigated. Moreover, the electrochemical properties of this modified electrode for determination of H_2O_2 is studied. Finally, this sensor has been used for the determination of the H_2O_2 amount in different real samples.

Experimental

Reagents and apparatus

H_2O_2 solution (30%), nafion, H_2SO_4 (98%), $KMnO_4$, HCl (37%), silver nitrate (99.8%), TBHQ and the other chemical reagents used for preparation of the buffer solutions were purchased from Merck and used as received. The phosphate buffer solutions (0.1 mol L^{-1}) were prepared with phosphoric acid and NaOH. GO was synthesized by the improved Hummers method.[19-21] Transmission electron microscopy (TEM) characterization of the graphene oxide nanosheets was performed using a microscope LEO 912AB. A droplet of graphene oxide dispersion was cast onto a TEM copper grid and the solvent was evaporated overnight at room temperature.

Electrochemical experiments were performed with a μ-Autolab potentiostat (Eco Chemie Utrecht) with GPES 4.9 software. The cell was equipped with a N-GO/AgNPs/TBHQ/GCE as a working electrode, a platinum electrode as an auxiliary electrode and a Ag/AgCl/3 mol L^{-1} KCl as a reference electrode. The pH measurement was performed with a Metrohm model 691 pH/mV meter. The morphological features and surface characteristics of the GO/AgNPs/TBHQ were studied using a scanning electron microscope (SEM) unit (HITACHI-3000 SH Model).

Preparation of modified electrodes

The working electrodes were prepared as following procedure. At first, GCE was carefully polished mechanically with 0.05 μm of Al_2O_3 slurry on a polishing cloth and then rinsed with doubly distilled water. After cleaning, it was immersed in a 0.1 mol L^{-1} sodium bicarbonate solution and was activated by a continuous potential cycling from −1.45 to 1.7 V at a sweep rate of 100 mV s^{-1}. According to the literature, during activation of the GCE surface, carboxyl and hydroxyl active groups are formed on the GCE surface.[22,23] Therefore, the existence of electronegative active atoms such as fluorine and oxygen on nafion, as well as the presence of carboxyl and hydroxyl groups on the GO, suggests that activation on the electrode surface result in formation of suitable interactions in order to better immobilize two compounds (GO and nafion) on the electrode surface.

For preparation of nafion-graphene oxide modified glassy carbon electrode (N-GO/GCE) 2 μL of a homogenized nafion-graphene oxide mixture (1 mg *per* 5 mL) was placed directly on to the activated GCE surface and dried at room temperature to form a graphene film at the GCE surface. Then, the N-GO/GCE was modified by a continuous potential cycling from −0.7 to 1.9 V at a sweep rate of 80 mV s^{-1} for 8 cycles in a solution containing 1 mmol L^{-1} $AgNO_3$ and 100 mmol L^{-1} nitric acid. As a final point, the modified electrode was rinsed with doubly distilled water and dried in air to give a silver nanoparticles modified N-GO/GCE (N-GO/AgNPs/GCE).[24] For the fabrication of N-GO/AgNPs/TBHQ/GCE, the N-GO/AgNPs/GCE was rinsed with doubly distilled water and was modified by 8 cycles of potential sweep between −230 and 70 mV at 20 mV s^{-1} in a 1.0 mmol L^{-1} solution of TBHQ in a 0.1 mol L^{-1} phosphate buffer solution (pH 7.0) (Scheme 1). The AgNPs/TBHQ/GCE was prepared by the same procedure for N-GO/AgNPs/TBHQ/GCE without graphene oxide. Moreover, TBHQ modified GCE (TBHQ/GCE) and N-GO/TBHQ/GCE were prepared by same procedure as N-GO/AgNPs/TBHQ/GCE preparation, but without graphene oxide and silver nanoparticles, and without silver nanoparticles, respectively. Before every cyclic voltammetry (CV) experiments, the elimination of oxygen was performed via nitrogen purge based on previously published protocol.[25]

Results and Discussion

TEM imaging results

Figure 1 shows TEM micrograph of a typical graphene oxide nanosheet deposited on a standard TEM grid. The

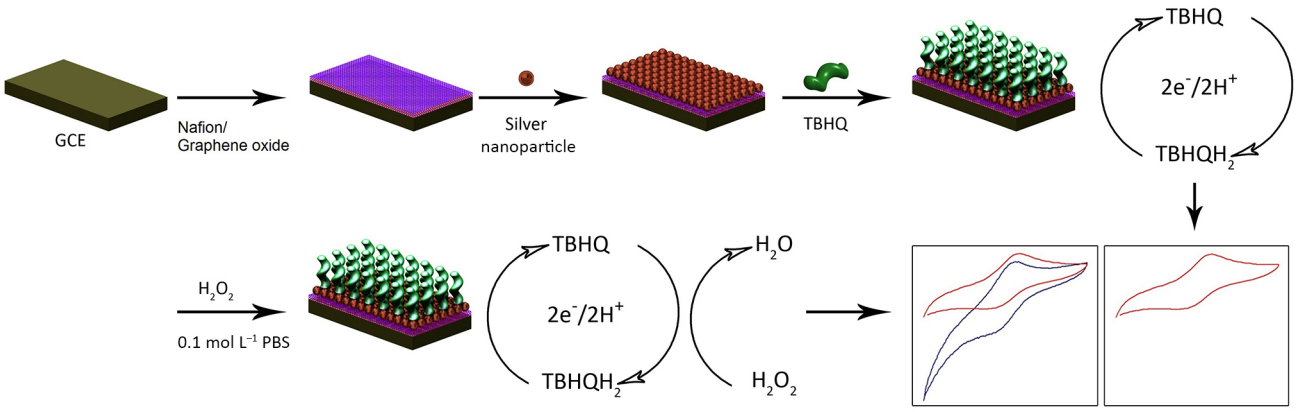

Scheme 1. Schematic diagram for the sensor fabrication and determination of H_2O_2.

sheet was several micrometers in dimension with the wrinkled (rough) surface texture. High-resolution TEM micrograph clearly illustrated the amorphous nature of the graphene oxide nanosheet.

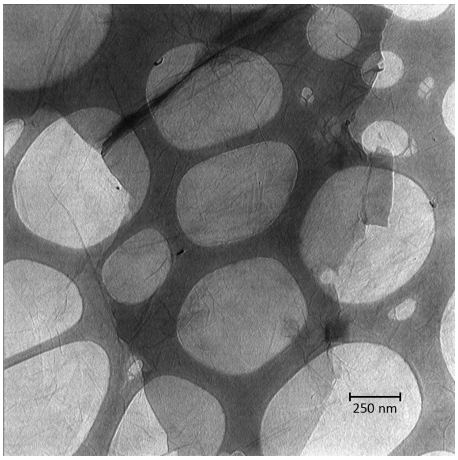

Figure 1. TEM image of synthesized graphene oxide nanosheets.

Electrochemical behavior of N-GO/AgNPs/TBHQ/GCE

The cyclic voltammograms obtained for N-GO/TBHQ/GCE (Figure 2a), AgNPs/TBHQ/GCE (Figure 2b), and N-GO/AgNPs/TBHQ/GCE (Figure 2c), at 20 mV s^{-1}, in 0.1 mol L^{-1} phosphate buffer solution (pH 7.0) containing no deliberately added electroactive materials, are depicted in Figure 2. As it can be seen, for N-GO/TBHQ/GCE (Figure 2a) and AgNPs/TBHQ/GCE (Figure 2b), with low peak currents, relatively high peak separations, low capacitance currents and for N-GO/AgNPs/TBHQ/GCE a pair of well-defined redox couple of TBHQ (Figure 2c) with high peak response, low peak potential separation and relatively high capacitance currents are observed, suggesting that the reversibility of TBHQ is significantly improved. Additionally, in order to provide a comparison, the sensor was prepared without addition of TBHQ onto the surface (Figure 2d). As it can be seen in Figure 2d, in absence of TBHQ (in our investigation potential range) there is no peak relating to redox of the agents and this observation can show properly that function of sensor by the immobilized TBHQ at the surface of N-GO/AgNPs/GCE. The increase of the peak currents and decrease of the peak potential separation for N-GO/AgNPs/TBHQ/GCE, indicate that the reversibility of TBHQ is improved at the N-GO/AgNPs surface. Also, we deduced that N-GO/AgNPs composition will increase the surface area of the modified electrode, so the background voltammetric response (capacitance current) and sensitivity of N-GO/AgNPs modified surface are higher than those for the N-GO, and AgNPs modified surfaces. Therefore, N-GO/AgNPs can be used as a new material for immobilizing and electron transfer reactions of TBHQ.

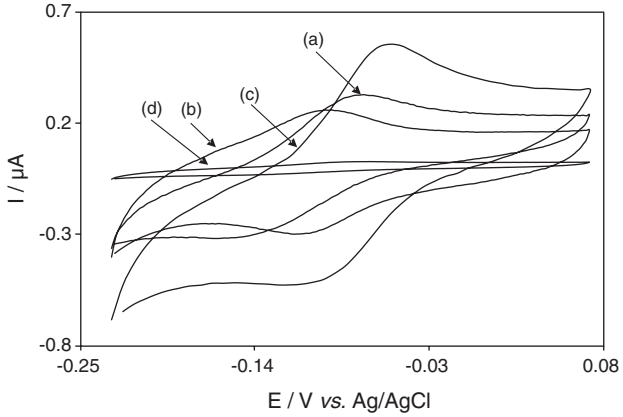

Figure 2. Cyclic voltammogram of (a) N-GO/AgNPs/TBHQ/GCE; (b) N-GO/TBHQ/GCE; (c) AgNPs/TBHQ/GCE; (d) N-GO/AgNPs/GCE in 0.1 mol L^{-1} phosphate buffer solution (pH 7.0).

Figure S1 (see Supplementary Information section), indicates the cyclic voltammograms of N-GO/AgNPs/TBHQ/GCE in a 0.1 mol L^{-1} phosphate buffer (pH 7.0) at various scan rates (5-95 mV s^{-1}). Figure S1a,

shows the anodic and the cathodic peak currents (I_{pa} and I_{pc}) values *versus* the potential scan rates. The linearity dependence indicates that the nature of the redox process is diffusion less controlled. Also, when the potential was scanned between −230 and 70 mV, a surface immobilized redox couple with a formal potential ($E^{0'}$) value of −83 mV was observed for N-GO/AgNPs/TBHQ/GCE. Moreover, the formal potential, $E^{0'}$, is almost independent of the potential scan rate for scan rates ranging from 5 to 150 mV s^{-1}, suggesting facile charge transfer kinetics over this range of scan rates. The studies on peak to peak potential separation ($\Delta E_p = E_{pa} - E_{pc}$) variation as a function of scan rate on the N-GO/AgNPs/TBHQ/GCE exhibit that ΔE_p is almost constant within the range of 5-150 mV s^{-1} (Figure S1b). At high scan rates, the separation between peak potentials increases with increasing scan rates (Figure S1c), indicating the limitation arising from charge transfer kinetics. The surface charge transfer rate constant, k_s, and the charge transfer coefficient, α, for the electron transfer between the electrodeposited TBHQ and N-GO/AgNPs were estimated from the variation of the oxidation and reduction peak potentials with the sweep rate according to the procedure of Laviron.[26] This theory predicts a linear dependence of E_p upon log ν for high scan rates, which can be used to extract the kinetic parameters of α and k_s from the slope and intercept of such plots, respectively. Transfer coefficient, α, can range from zero to one, which is as an indicator of the symmetry of the barrier to reaction.[27] The large value of k_s indicates that the charge transfer rate on the surface of N-GO/AgNPs/TBHQ/GCE is high. From the values of ΔE_p corresponding to different potential scan rates of 900-3000 mV s^{-1}, an average value of k_s and α were obtained, 6.15 ± 0.150 s^{-1} and 0.52, respectively. The obtained k_s value is higher than the previously reported values for other works such as k_s = 6.3 and 6.0 s^{-1}.[28]

Characterization of the surface morphology of N-GO/AgNPs/TBHQ/GCE

The surface morphologies of different electrodes were characterized by SEM, since the morphology was also related to the performance of the electrode. Figure 3 shows the morphologies of N-GO/AgNPs/GCE (Figure 3a) and N-GO/AgNPs/TBHQ/GCE (Figure 3b). Figure 3a shows that AgNPs is successfully immobilized on the electrode surface of N-GO/GCE after electrochemical deposition. Figure 3b shows that TBHQ has been completely immobilized on the electrode surface of N-GO/AgNPs/GCE.

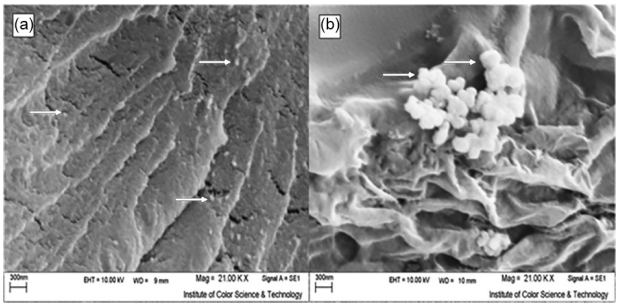

Figure 3. SEM images of (a) N-GO/AgNPs/GCE; (b) N-GO/AgNPs/TBHQ/GCE.

Electrocatalytic reduction of H_2O_2 at the N-GO/AgNPs/TBHQ/GCE

In order to test the electrocatalytic activity of the N-GO/AgNPs/TBHQ/GCE, the cyclic voltammograms at N-GO/TBHQ/GCE (Figure 4A), AgNPs/TBHQ/GCE (Figure 4B), and N-GO/AgNPs/TBHQ/GCE (Figure 4C) were obtained in the absence and presence of 0.3 mmol L^{-1} of H_2O_2. Afterwards, the results were compared with the cyclic voltammogram of N-GO/TBHQ/GCE (Figure 4A, curve a), AgNPs/TBHQ/GCE (Figure 4B, curve a) and N-GO/AgNPs/TBHQ/GCE (Figure 4C, curve a) in supporting electrolyte at pH 7.0. A comparison of the peak potential of the cyclic voltammograms of the N-GO/AgNPs/TBHQ/GCE in the presence of H_2O_2 (Figure 4C, curve b) with the peak potentials of the modified electrode in the supporting electrolyte (pH 7.0) (Figure 4C, curve a) illustrates that, after the addition of H_2O_2, a drastic enhancement occurs in the cathodic peak current, and a very small current is observed in the anodic scan. This behavior is consistent with a very strong electrocatalytic effect. Similar results are observed for N-GO/TBHQ/GCE and AgNPs/TBHQ/GCE in a 0.1 mol L^{-1} phosphate buffer solution (pH 7.0) in the absence (Figure 4A, curve a and Figure 4B, curve a), and the presence of 0.3 mmol L^{-1} H_2O_2 (Figure 4A, curve b and Figure 4B, curve b). But, as it can be seen, at N-GO/AgNPs/TBHQ/GCE, the reduction of H_2O_2 gives rise to a typical electrocatalytic response at −97 mV (Figure 4C, curve b), with an cathodic peak current that is greatly enhanced over that observed for the AgNPs/TBHQ/GCE (Figure 4B, curve b), and N-GO/TBHQ/GCE (Figure 4A, curve b).

In addition, the cathodic peak potential for the reduction of H_2O_2 at N-GO/AgNPs/TBHQ/GCE (Figure 4A, curve b), is at −97 mV, while at AgNPs/TBHQ/GCE (Figure 4B, curve b) and N-GO/TBHQ/GCE (Figure 4C, curve b), H_2O_2 is reduced at the potential of −109 and −142 mV, respectively. So, a decrease in the over-potential and a

dramatic enhancement of the peak current occur for H_2O_2 at the N-GO/AgNPs/TBHQ/GCE surface. Indeed, in the first step the immobilized TBHQ at the surface of electrode participates in oxidation reaction in positive potentials and converts to TBQ, therefore, at the beginning of cyclic voltammograms all the immobilized TBHQ converts to TBQ which these TBQ at the potential of −97.0 mV (Figure 4, curve a) leads to cathodic current. In reverse cycle the formed TBHQ at the surface of electrode converts to TBQ by applying potential of −55.0 mV and anodic current observes. Figure 4 (curve a) shows the process of redox reaction TBHQ. The equation 1 is mentioned as semi reversible electrochemical reaction (E_r). While in the presence of H_2O_2 by applying cathodic potential TBQ converts to TBHQ. Some of generated TBHQ at the surface of electrode with H_2O_2 participates in oxidation process and again converts to TBQ. Based on equation 2, generated TBQ at the surface of electrode participates in reduction process and leads to increase in cathodic current. On the other hand some of TBHQ oxidized in this step and, therefore, in reverse step, by decreasing the amount of TBHQ, anodic current decreases towards the previous step (absence of H_2O_2). This mechanism is "E_rC_i"' based on mentioned concepts. Thus, based on this result, the catalytic mechanism can be expressed as shown in equations 1 and 2.

$$TBQ + 2e + 2H^+ \rightleftharpoons TBHQ \qquad (E_r) \quad (1)$$

$$2\ TBHQ + H_2O_2 \rightleftharpoons 2TBQ + 2H_2O \quad (C_i) \quad (2)$$

The data obtained clearly indicate that the combination of TBHQ, N-GO and AgNPs definitely improve the characteristics of H_2O_2 reduction. The electrocatalytic reduction characteristics of H_2O_2 at various modified electrode surfaces at pH 7.0 are summarized in Table S1 (see Supplementary Information section).

The effect of scan rate on the electrocatalytic reduction of H_2O_2 at the N-GO/AgNPs/TBHQ/GCE was investigated at various scan rates by cyclic voltammetry in a 0.1 mol L^{-1} phosphate buffer solution (pH 7.0) containing 0.30 mmol L^{-1} H_2O_2. The plot of peak current (I_p) against square root of scan rate ($v^{1/2}$), in range of 6-24 mV s^{-1} (Figure S2a), was found to be linear, suggesting that at sufficient over-potential the process is diffusion rather than surface controlled. These results exhibit that the overall electrochemical reduction of H_2O_2 at the modified electrode might be controlled by a cross-exchange process operating between the redox site of N-GO/AgNPs/TBHQ/GCE and the diffusion of H_2O_2. For such mechanism and derived a relationship between the peak current and the concentration of the substrate for a case of a slow scan rate, v, and a large catalytic rate constant, k', which is the catalytic rate constant between N-GO/AgNPs/TBHQ/GCE and H_2O_2, thus, this value of k' explains a good catalytic feature for the oxidation of H_2O_2 at N-GO/AgNPs/TBHQ/GCE. The higher k' value shows higher rate of electron transfer and with the increase in rate of electron transfer the cathodic peak current and sensitivity of determination would be increased. Andrieux and Saveant[29] developed a theoretical model for a heterogeneous catalysis:

$$I_{cat} = 0.49nFAC_b(nFADv/RT)^{1/2} \qquad (3)$$

where D and C_b are the diffusion coefficient (2.02×10^{-6} cm^2 s^{-1} obtained by chronoamperometry) and the bulk concentration (mol cm^{-3}) of H_2O_2. Low values of k' result in values lower than 0.496 for the constant. The value of this constant was found to be 0.27 for N-GO/AgNPs/TBHQ/GCE, in the presence of 0.3 mmol L^{-1} of H_2O_2 for low scan rates (6-24 mV s^{-1}). According

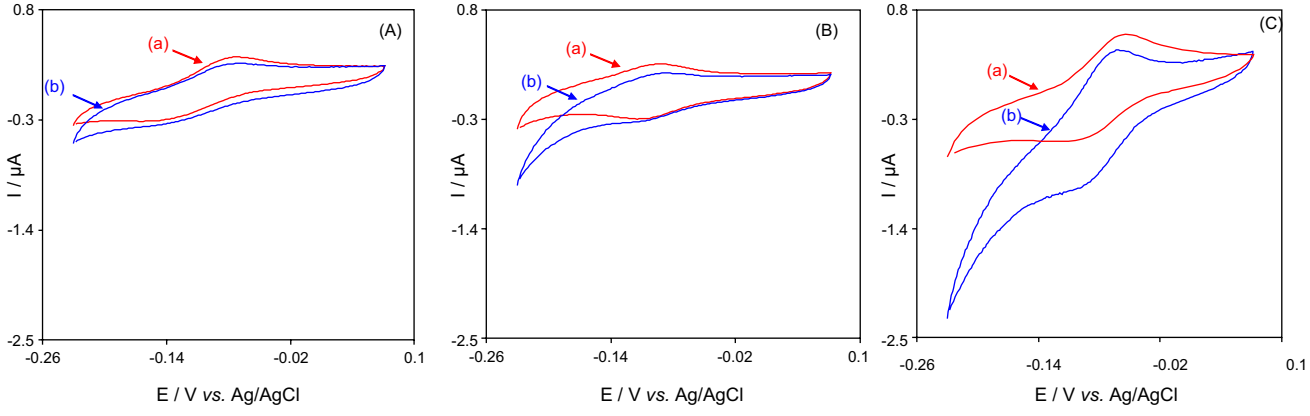

Figure 4. Cyclic voltammograms in 0.1 mol L^{-1} phosphate buffer solution (pH 7.0) at scan rate 20 mV s^{-1} in the absence (curves a) and presence of 0.3 mmol L^{-1} H_2O_2 (curves b). (A) N-GO/TBHQ/GCE; (B) AgNPs/TBHQ/GCE; (C) N-GO/AgNPs/TBHQ/GCE.

to the approach of Andrieux and Saveant and using Figure 1 in their theoretical paper,[29] an average value of k' = 8.2 (± 0.25) × 10^{-4} cm s^{-1} was obtained. This value is comparable with k' = 4.7 (± 0.03) × 10^{-4},[25] k' = 1.17 (± 0.04) × 10^{-3} and k' = 4.96 (± 0.004) × 10^{-4},[30] k' = 1.3 (± 0.20) × 10^{-3},[31] k' = 6.25 (± 0.15) × 10^{-4},[32] k' = 1.1 (± 0.036) × 10^{-3},[33] k' = 1.2 (± 0.03) × 10^{-3} cm s^{-1},[24] previously reported for different analytes.

The number of electrons in the overall reaction, n, can be obtained from the plot slope of I_P *versus* $v^{1/2}$ (Figure S2a). According to the following equation for a totally irreversible diffusion controlled processes:[27]

$$I_p = 3.01 \times 10^5 n[(1 - \alpha)n_\alpha]^{1/2} A C_b D^{1/2} v^{1/2} \quad (4)$$

Considering $(1 - \alpha)n_\alpha = 0.68$ (see below), D = 2.02 × 10^{-6} cm^2 s^{-1} (which is obtained by chronoamperometry) and A = 0.0314 cm^2, it is estimated that the total number of electrons involved in the cathodic reduction of H_2O_2 is n = 1.87 ca. 2.

Linear sweep voltammograms at different potential scan rates of N-GO/AgNPs/TBHQ/GCE in a 0.1 mol L^{-1} phosphate buffer (pH 7.0) containing 0.30 mmol L^{-1} H_2O_2 are depicted in inset of Figure S2b. This part of the voltammogram, known as Tafel region, is affected by electron transfer kinetics between the H_2O_2 and the surface confined N-GO/AgNPs/TBHQ/GCE. In this condition, the number of electrons involved in the rate determining step can be estimated from the slope of the Tafel plot (inset of Figure S2b).[27] The Tafel plots were drawn using points of the Tafel region of the linear sweep voltammograms in Figure S2. In this work, an average value of 0.32 ± 0.01 is obtained for the kinetic parameter of the anodic charge transfer coefficient, α_a, assuming the rate determining step of the electron transfer process between H_2O_2 and the modified electrode contained one electron (n_α = 1).

Furthermore, chronoamperometry in pH 7.0 phosphate buffer (0.1 mol L^{-1}) containing different concentrations of H_2O_2 was applied at N-GO/AgNPs/TBHQ/GCE to estimate the diffusion coefficient, D, of H_2O_2. Figure S3, show the chronoamperograms obtained at a potential step of −150 mV. For an electroactive material (H_2O_2 in this case) with a diffusion coefficient of D, the current observed for the electrochemical reaction at the mass transport limited conditions described by the Cottrell equation.[27] Under diffusion control, a plot of I *versus* $t^{-1/2}$ will be linear, and from the slope the value of D can be obtained. Figure S3a shows the experimental plots with the best fits for different concentrations of H_2O_2 employed. The slopes of the resulting straight lines were then plotted *versus* the H_2O_2 concentration (Figure S3, inset b), from whose slope we calculated a diffusion coefficient of 2.02 × 10^{-6} cm^2 s^{-1}.

Differential pulse voltammetric studies

Differential pulse voltammetry, DPV, has a much higher current sensitivity than cyclic voltammetry, and it can be used to determine the linear range and to estimate the detection limit of H_2O_2. Figure 5 shows the voltammetric response of N-GO/AgNPs/TBHQ/GCE to different H_2O_2 concentrations. Voltammograms clearly show that the plot of peak current *vs.* H_2O_2 concentration is formed of three linear segments with different slopes (slope: −6 × 10^{-5} μA (μmol L^{-1})$^{-1}$ for first linear segment, −6 × 10^{-4} μA (μmol L^{-1})$^{-1}$ for second linear segment and −41 × 10^{-4} μA (μmol L^{-1})$^{-1}$ for third linear segment), corresponding to three different ranges of substrate concentration (1.52-9.79 μmol L^{-1} for first linear segment, 9.79-231.0 μmol L^{-1} for second linear segment and 231.0-8330.0 μmol L^{-1} for third linear segment). A comparison of the sensitivities (slopes of the calibration plots) of the three linear segments shows a decrease of sensitivity in the second and third linear range probably due to the electron transfer kinetic limitation between the analyte and the modified electrode surface. The calibration plot, in the range of 1.52-9.79 μmol L^{-1} H_2O_2, was used to estimate the lower limit of detection of H_2O_2 at N-GO/AgNPs/TBHQ/GCE. According to the method mentioned in the references,[34] the lower detection limit, C_m, was obtained to be 0.46 μmol L^{-1} by using the equation $C_m = 3s_{bl}/m$, where s_{bl} is the standard deviation of the blank response (μA) and m is the slope of the calibration plot (−41 × 10^{-4} μA (μmol L^{-1})$^{-1}$).

The average voltammetric peak current and the precision estimated in terms of the coefficient of variation for repeated measurements (n = 15) of 5.0 μmol L^{-1} H_2O_2 at N-GO/AgNPs/TBHQ/GCE were −0.382 ± 0.013 μA and 2.6%, respectively. This coefficient of variation value indicates that N-GO/AgNPs/TBHQ/GCE is stable and does not undergo surface fouling during the voltammetric measurements. A comparison of the analytical performance of N-GO/AgNPs/TBHQ/GCE for electrocatalytic reduction of H_2O_2 with other sensors is presented in Table 1.

The results of Table 1 show that these values are comparable with values reported by other research groups. As it can be seen in Table 1, the present work in comparison to all the manuscripts listed below (except reference 38) has wider linear range. About the detection limit, in comparison to the mentioned works in Table 1, except the references 39, 40 and 41, has the lowest detection limit, but the presented nanosensor is more simple and inexpensive.

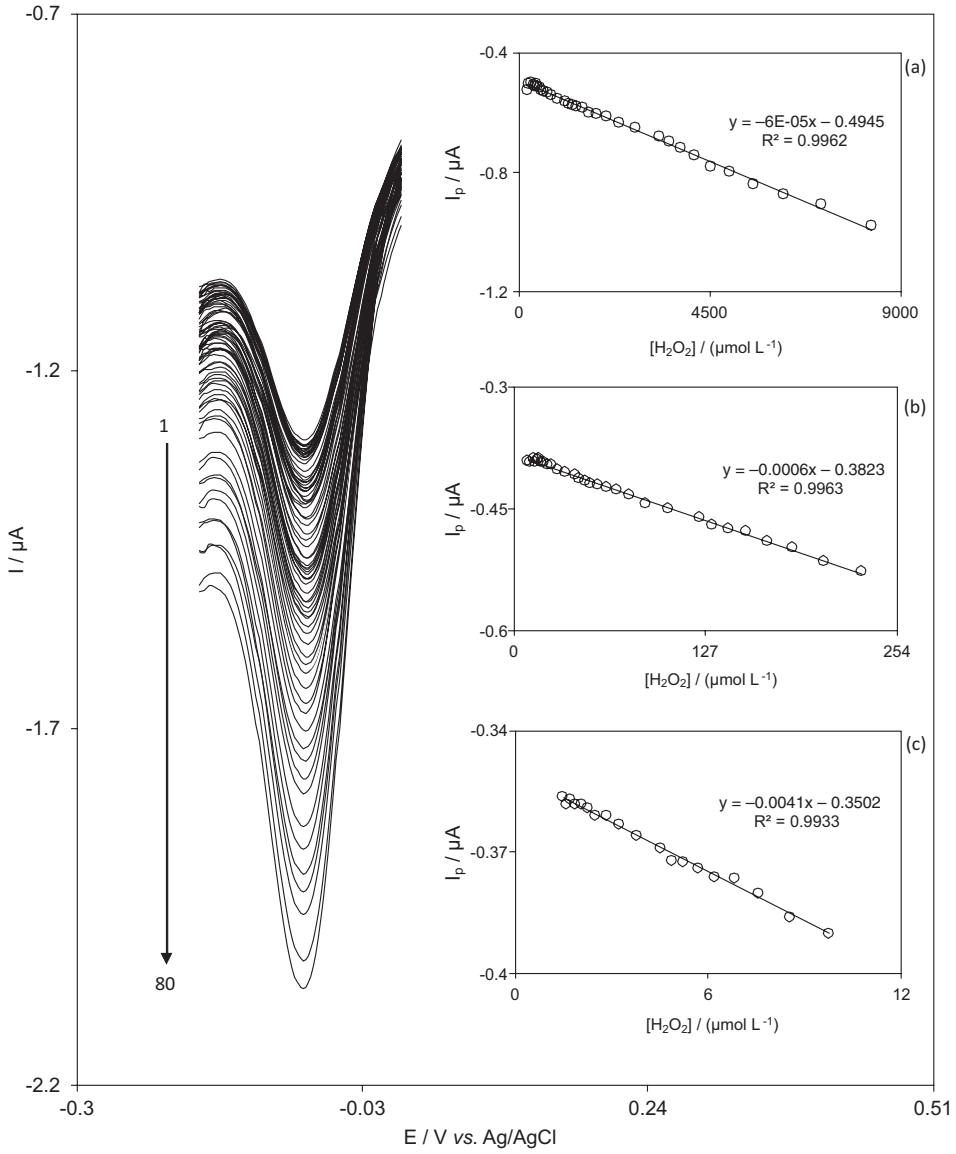

Figure 5. Differential pulse voltammograms of an N-GO/AgNPs/TBHQ/GCE in 0.1 mol L^{-1} phosphate buffer solution (pH 7.0) containing different concentrations of hydrogen peroxide. The numbers of 1-80 correspond to 1.52-83.3 × 10^2 µmol L^{-1} hydrogen peroxide. Insets show the plots of the electrocatalytic peak current, corrected for any residual current, as a function of hydrogen peroxide concentration in the range of (a) 231.0-8330.0 µmol L^{-1}; (b) 9.79-231.0 µmol L^{-1}; (c) 1.52-9.79 µmol L^{-1}.

In addition, to estimate the repeatability of the nanosensor, the response of modified electrode toward determination of H_2O_2 in period of time were investigated daily. The modified electrodes were utilized by the described method in the Experimental section for determination of different solution of 20 µmol L^{-1} H_2O_2 with differential pulse voltammetry method. By assuming relative standard deviation, RSD = 5%, the prepared modified electrode has proper stability for about 14 days. While the utilized electrode after determination of H_2O_2 has just stability for about 3 days. Based on this, it is recommend to remodify the electrode in order to determine H_2O_2 with high sensitivity.

Determination of hydrogen peroxide in beverages and milk

From the results that are mentioned in the previous section, it is apparent that N-GO/AgNPs/TBHQ/GCE has a good detection limit and high sensitivity to H_2O_2 determination in real samples. The modified electrode was used to measure H_2O_2 in some beverages in order to test its practical application. For this purpose 5 mL of different beverages sample and milk was diluted to 10 mL with a 0.1 mol L^{-1} phosphate buffer solution (pH 7.0). Then, certain amounts of H_2O_2 were added and their recovery was determined by differential pulse voltammetry. The results were obtained using the proposed method and

Table 1. Comparison of some analytical parameters of the several modified electrodes for H_2O_2 determination

Sensor component	Method	Linear range / (μmol L^{-1})	Detection limit / (μmol L^{-1})	Reference
GNPs/GN-CS[a]	amperometry	5-35000	1.6	35
Gel-MWCNTs/Cat/GAD[b]	amperometry	200-5000	1	36
AgND/rGO/GCE[c]	RDE (6000 rpm)	0.05-30	10	37
Cu_2O/N-graphene/Nafion[d]	amperometry	5-3570	0.8	38
Pt NPs/NPG[e]	amperometry	0.1-20	0.072	39
Cu_2O/Cu nanocomposite	amperometry	0.4-10000	0.2	40
(HRP-Pd)/f-graphene-Gr[f]	amperometry	25-3500	0.05	41
Hollow AuNPs/CNTs/SPAN[g]	amperometry	5-225 225-8825	0.4	42
MnO_2 nanosheet/graphene	amperometry	10-90 200-900	2	43
AgNPs-GO[h]	amperometry	20000-10	0.5	44
PB/NPGF[i]	amperometry	1-10 10-100	0.36	45
PB/Au-Chit/MCNTs[j]	amperometry	3.98-19.61	3.36	46
PB/POPD[k]	amperometry	0.1-120	0.05	47
N-GO/AgNPs/TBHQ[l]	DPV[m]	1.52-9.79 9.79-231.0 231.0-8330.0	0.46	this work

[a]GNPs/GN-CS: gold nanoparticles-graphene-chitosan; [b]gel-MWCNTs/Cat/GAD: gelatin-multiwalled carbon nanotubes-catalase-glutaraldehyde; [c]AgND/rGO/GCE: silver nanodendrite-reduced graphene oxide-glassy carbon electrode; [d]Cu_2O/N-graphene/nafion: Cu_2O-nitrogen-doped graphene-nafion; [e]Pt NPs/NPG: Pt nanoparticles-nanoporous gold; [f](HRP-Pd)/f-graphene-Gr: horseradish peroxidase-palladium/functionalized-graphene modified graphite; [g]hollow AuNPs/CNTs/SPAN: hollow gold nanoparticles/carbon nanotube/self-doped polyaniline; [h]AgNPs-GO: silver nanoparticles-graphene oxide; [i]PB/NPGF: prussian blue modified nanoporous gold film; [j]PB/Au-Chit/MCNTs: Prussian Blue modified gold-chitosan nanoparticle/multiwall carbon nanotubes; [k]PB/POPD: Prussian Blue and poly(*o*-phenylenediamine) (POPD); [l]N-GO/AgNPs/TBHQ: nafion/graphene oxide/silver nanoparticles/tertiary butylhydroquinone (TBHQ); [m]DPV: differential pulse voltammetry.

Table 2. Determination of H_2O_2 in six commercial beverages using N-GO/AgNPs/TBHQ/GCE

Beverage sample	Added / (μmol L^{-1})			Found / (μmol L^{-1})			Recovery (n = 3) / %		
Apple juice	2.000	4.000	6.000	2.050	4.080	5.930	102.5	102.0	98.80
Orange juice	3.000	6.000	9.000	3.060	5.950	8.960	1020.0	99.12	99.50
Peach juice	3.000	6.000	9.000	3.030	5.950	9.040	101.0	99.17	100.4
Pineapple juice	2.000	4.000	6.000	2.020	4.010	6.030	101.0	100.2	100.5
Strawberry juice	2.500	5.000	7.500	2.470	5.030	7.520	98.80	100.6	100.3
Pomegranate juice	3.000	6.000	9.000	3.010	6.030	8.970	100.3	100.5	99.70
Milk sample 1	2.000	5.000	7.000	2.033	5.005	7.012	101.65	100.10	100.17
Milk sample 2	3.000	4.000	6.000	3.006	3.998	5.995	100.2	99.95	99.91
Milk sample 3	3.000	6.000	9.000	2.910	6.007	9.018	97	100.1	100.2

certified with a calibration graph of H_2O_2 inside the range of 1.52-9.79 μmol L^{-1}. The outcome (Table 2) show that the recoveries are in the range of 97.00 to 102.5%.

Conclusions

Based on the results obtained in this manuscript, it is concluded that the composition of N-GO and AgNPs at the surface of GCE can increase background voltammetric response (capacitance current) and sensitivity of TBHQ. Therefore, the N-GO/AgNPs/TBHQ/GCE is fabricated and then used as a new sensor for electrocatalytic reduction of H_2O_2. This modified electrode exhibits an electrocatalytic behavior to H_2O_2 reduction at a much lower over potential compared with the N-GO/TBHQ/GCE and AgNPs/TBHQ/GCE. The average values $8.2 (\pm 0.25) \times 10^{-4}$ cm s^{-1} and 0.32 ± 0.01 were obtained for the heterogeneous electron transfer rate constant, k', and the charge transfer coefficient, α, between the adsorbed TBHQ layer and H_2O_2. The diffusion coefficient of H_2O_2 was calculated as 2.02×10^{-6} cm^2 s^{-1} using chronoamperometric results. The calibration curves for H_2O_2 determination

were obtained in the ranges of 1.52-9.79, 9.79-231.0 and 231.0-8330.0 μmol L^{-1} with differential pulse voltammetry. Moreover, the proposed modified electrode was very useful for accurate determination of H_2O_2 in real samples.

Supplementary Information

Supplementary data (cyclic voltammetric and chronoamperometric responses of N-GO/AgNPs/TBHQ/GCE) are available free of charge at http://jbcs.sbq.org.br as PDF file.

Acknowledgments

The authors would like to kindly acknowledge all the supports and funding from Islamic Azad University of Yazd.

References

1. Eskandani, M.; Hamishehkar, H.; Dolatabadi, J. E. N.; *Food Chem.* **2014**, *153*, 315.
2. Shahabadi, N.; Maghsudi, M.; Kiani, Z.; Pourfoulad, M.; *Food Chem.* **2011**, *124*, 1063.
3. Jia, F.; Zhong, H.; Zhu, F.; Li, X.; Wang, Y.; Cheng, Z.; Zhang, L.; Sheng, Z.; Guo, L.; *Electroanalysis* **2014**, *26*, 2244.
4. Ensafi, A. A.; Jafari-Asl, M.; Rezaei, B.; *Talanta* **2013**, *103*, 322.
5. Alpat, S.; Alpat, S. K.; Dursun, Z.; Telefoncu, A.; *J. Appl. Electrochem*. **2009**, *39*, 971.
6. Kurowska-Tabor, E.; Jaskula, M.; Sulka, G. D.; *Electroanalysis* **2014**, *27*, 1968.
7. Tsaplev, Y. B.; *J. Anal. Chem*. **2012**, *67*, 506.
8. Steinberg, S. M.; *Environ. Monit. Assess.* **2013**, *185*, 3749.
9. Vasicek, O.; Papezikova, I.; Hyrsl, P.; *Eur. J. Entomol.* **2011**, *108*, 481.
10. Odo, J.; Inoguchi, M.; Ohira, S.; Tsukikawa, S.; Aramaki, M.; Matsuhama, S.; Taito, M.; Takayama, A.; *Anal. Sci.* **2013**, *29*, 1041.
11. Liu, H.; Chen, X.; Huang, L.; Wang, J.; Pan, H.; *Electroanalysis* **2014**, *26*, 556.
12. Salimi, A.; Mahdioun, M.; Noorbakhsh, A.; Abdolmaleki, A.; Ghavami, R.; *Electrochim. Acta* **2011**, *56*, 3387.
13. Won, Y. H.; Huh, K.; Stanciu, L. A.; *Biosens. Bioelectron.* **2011**, *26*, 4514.
14. Khan, M. M.; Ansari, S. A.; Lee, J.; Cho, M. H.; *Mater. Sci. Eng., C* **2013**, *33*, 4692.
15. Han, Y.; Zheng, J.; Dong, S.; *Electrochim. Acta* **2013**, *90*, 35.
16. Gao, H.; Qi, X.; Chen, Y.; Sun, W.; *Anal. Chim. Acta* **2011**, *704*, 133.
17. Jia, M.; Wang, T.; Liang, F.; Hu, J.; *Electroanalysis* **2012**, *24*, 1864.
18. Wang, F.; Zhou, J.; Liu, Y.; Wu, S.; Song, G.; Ye, B.; *Analyst* **2011**, *136*, 3943.
19. Chen, J.; Yao, B.; Li, C.; Shi, G.; *Carbon* **2013**, *64*, 225.
20. Hummers Jr., W. S.; Offeman, R. E.; *J. Am. Chem. Soc.* **1958**, *80*, 1339.
21. Marcano, D. C.; Kosynkin, D. V.; Berlin, J. M.; Sinitskii, A.; Sun, Z.; Slesarev, A.; Alemany, L. B.; Lu, W.; Tour, J. M.; *ACS Nano* **2010**, *4*, 4806.
22. Pariente, F.; Lorenzo, E.; Abruna, H. D.; *Anal. Chem.* **1994**, *66*, 4337.
23. Zare, H. R.; Samimi, R.; Nasirizadeh, N.; Mazloum-Ardakani, M.; *J. Serb. Chem. Soc*. **2010**, *75*, 1434.
24. Nasirizadeh, N.; Aghayizadeh, M. M.; Bidoki, S. M.; Yazdanshenas, M. E.; *Int. J. Electrochem. Sci.* **2013**, *8*, 11264.
25. Nasirizadeh, N.; Hajihosseini, S.; Shekari, Z.; Ghaani, M.; *Food Anal. Methods* **2015**, *8*, 1546.
26. Laviron, E.; *J. Electroanal. Chem.* **1979**, *101*, 19.
27. Bard, A. J.; Faulkner, L. R.; *Electrochemical Methods, Fundamentals and Applications*; Wiley: New York, 2001.
28. Nasirizadeh, N.; Shekari, Z.; Tabatabaee, M.; Ghaani, M.; *J. Braz. Chem. Soc.* **2015**, *26*, 713.
29. Andrieux, C. P.; Saveant, J. M.; *J. Electroanal. Chem.* **1978**, *93*, 163.
30. Nasirizadeh, N.; Shekari, Z.; Zare, H. R.; Shishehbore, M. R.; Fakhari, A. R.; Ahmar, H.; *Biosens. Bioelectron.* **2013**, *41*, 608.
31. Nasirizadeh, N.; Shekari, Z.; *Ionics* **2014**, *20*, 275.
32. Aghayizadeh, M. M.; Nasirizadeh, N.; Bidoki, S. M.; Yazdanshenas, M. E.; *Int. J. Electrochem. Sci.* **2013**, *8*, 8848.
33. Nasirizadeh, N.; Shekari, Z.; Zare, H. R.; Ardakani, S. A. Y.; Ahmar, H.; *J. Braz. Chem. Soc.* **2013**, *24*, 1846.
34. Skoog, D. A.; Holler, F. J.; Crouch, S. R.; *Principles of Instrumental Analysis*; Thomson Brooks/Cole: London, 2007.
35. Jia, N.; Huang, B.; Chen, L.; Tan, L.; Yao, S.; *Sens. Actuators, B* **2014**, *195*, 165.
36. Wang, Y.; Li, T.; Zhang, W.; Huang, Y.; *J. Solid State Electrochem*. **2014**, *18*, 1981.
37. Sawangphruk, M.; Sanguansak, Y.; Krittayavathananon, A.; Luanwuthi, S.; Srimuk, P.; Nilmoung, S.; Maensiri, S.; Meevasana, W.; Limtrakul, J.; *Carbon* **2014**, *70*, 287.
38. Jiang, B. B.; Wei, X. W.; Wu, F. H.; Wu, K. L.; Chen, L.; Yuan, G. Z.; Dong, C.; Ye, Y.; *Microchim. Acta* **2014**, *181*, 1463.
39. Yin, G.; Xing, L.; Ma, X. J.; Wan, J.; *Chem. Pap.* **2014**, *68*, 435.
40. Luo, B.; Li, X.; Yang, J.; Li, X.; Xue, L.; Li, X.; Gu, J.; Wang, M.; Jiang, L.; *Anal. Methods* **2014**, *6*, 1114.
41. Nandini, S.; Nalini, S.; Manjunatha, R.; Shanmugam, S.; Melo, J. S.; Suresh, G. S.; *J. Electroanal. Chem.* **2013**, *689*, 233.
42. Chen, X.; Guo, B.; Hu, P.; Wang, Y.; *Electroanalysis* **2014**, *26*, 1513.
43. Xiaomiao, F.; Zhang, Y.; Song, J.; Chen, N.; Zhou, J.; Huang, Z.; Ma, Y.; Zhang, L.; Wang, L.; *Electroanalysis* **2015**, *27*, 353.

44. Jun, Z.; KeunSoo, K.; Zhenxian, L.; Huan, F.; Shifeng, H.; *Electroanalysis* **2014**, *26*, 251.
45. Ghaderi, S.; Ayatollahi Mehrgardi, M.; *Bioelectrochem*. **2014**, *98*, 64.
46. Li, M.; Zhao, G.; Yue, Z.; Huang, S.; *Microchim. Acta* **2009**, *167*, 167.
47. Ping, J.; Wu, J.; Fan, K.; Ying, Y.; *Food Chem*. **2011**, *126*, 2005.

Submitted: September 24, 2015
Published online: February 2, 2016